Available online at www.sciencedirect.com
ScienceDirect
Journal of Power Sources 159 (2006) 595–604
JOURNAL OF POWER SOURCES
www.elsevier.com/locate/jpowsour

Flow maldistribution in interdigitated channels used in PEM fuel cells☆

K.B. Shyam Prasad, S. Maharudrayya, S. Jayanti*

Department of Chemical Engineering, Indian Institute of Technology Madras, Chennai 600 036, India

Received 5 September 2005; accepted 30 September 2005
Available online 4 January 2006

Abstract

The interdigitated flow configuration is unique in the sense that the reactants are forced through the porous electrodes in this configuration, whereas this occurs by diffusion in the conventional types of flow fields. Previous studies have shown that this reduces the possibility of flooding of the cathode electrode resulting in improved efficiency of the fuel cell, however, at the cost of a higher-pressure drop. In the present study, computational fluid dynamics (CFD)-based simulations have been used to study the effect of important geometric parameters such as the channel, the header and the electrode dimensions. The results show that for low permeabilities the flow is uniform across the porous electrode; however, for permeabilities in the range of 10^{-11} to 10^{-10} m^2, the flow may become non-uniform. Under these conditions, calculations in four-cell and eight-cell parallel interdigitated configuration show that significant flow maldistribution among the parallel channels is likely to occur.

Keywords: PEM fuel cells; Flow maldistribution; Interdigitated channels

1. Introduction

Fuel cell devices offer technical and environmental advantages such as high performance characteristics, reliability, durability and clean power when compared to conventional thermal power systems. Polymer Electrolyte Membrane (PEM) fuel cells, which operate at low temperatures (around 80 °C), have a theoretical efficiency which is much greater than that of conventional internal combustion (IC) engines, quick start-up compared to other fuel cells operating at high temperature and zero toxic emissions if hydrogen is available. Thus, they offer an attractive alternative to IC engines for transportation applications. For achieving high efficiency, PEM fuel cells have to overcome three major resistances, viz. activation polarization—because of the energy intensive activity of the making and breaking of chemical bonds at the cathode and the anode; ohmic polarization—caused by electrical losses in the cell; and concentration polarization resulting from restrictions to the transport of the fuel gases to the reaction sites. By decreasing these resistances (polarization losses), the efficiency of the fuel cell can be increased. However, decreasing the activation or the ohmic losses is difficult as they both inherent resistances. Much effort has been spent in recent years in decreasing the resistance to transport of the reactants/products in the PEM fuel cell. A number of flow channel configurations have been proposed [1,2] to reduce the mass transfer limitation occurring at high current densities.

The various channel configurations typically studied can be seen as combinations of parallel and serpentine configurations. Predictive models to calculate the pressure drop and flow distribution in several of these have been developed recently by the present authors [3,4]. Nguyen [5] has proposed a rather unique flow configuration called the interdigitated flow configuration (see Fig. 1), in which the reactants and the products forced to pass through the porous electrodes on their way to or from the membrane–electrode-assembly (MEA) where the reactions take place. Although this flow passage involves flow through a porous medium and therefore a large pressure drop, it has been reported to have excellent flooding resistance and higher current densities can be realized in this configuration [6]. Also, the reactants pass through the porous electrodes by convection rather than by diffusion alone. This increases the concentration of the reactants at the reaction sites, which in turn decreases the resistance to concentration polarization.

Several theoretical and experimental studies have been carried out on interdigitated flow fields [5–12]. Yi and Nguyen [7]

☆ This paper was presented at the 2005 Fuel Seminar, PALM Springs, CA, USA.

* Corresponding author. Tel.: +91 44 2257 4168; fax: +91 44 2235 0509.
E-mail address: sjayanti@iitm.ac.in (S. Jayanti).

0378-7753/$ – see front matter © 2005 Published by Elsevier B.V.
doi:10.1016/j.jpowsour.2005.09.066

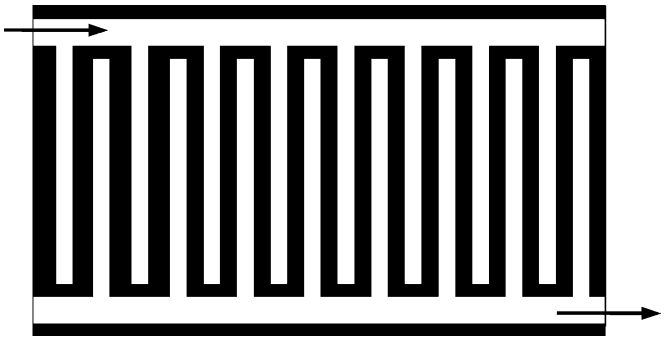

Fig. 1. Schematic diagram of interdigitated flow field.

presented a two-phase flow model for PEM fuel cell, with an interdigitated flow field and extended it to account for the effect of inert species such as nitrogen and water vapour. He et al. [8] presented an extension of the model of Yi and Nguyen [7] for two phase and two-dimensional flow. De Souza and Gonzalez [9] carried out comparative studies on the fuel cell performance of parallel, serpentine and interdigitated flow fields. Wang and Liu [10] carried out experiments to study the effect of cell temperature, gas humidification, cell operating pressure and reactant gas flow rate on the performance of a proton exchange membrane fuel cell with interdigitated flow fields. Hu et al. [11] presented a three-dimensional model of conventional and interdigitated flow fields. Grujicic et al. [12] developed a three-dimensional model coupled to a constrained non-linear optimization technique to optimize the geometrical parameters of the cathode such as the air inlet pressure, the cathode thickness and length and the width of shoulders in the interdigitated air distributor for a PEM fuel cell.

The above studies indicate an improved performance of the PEM fuel cell with an interdigitated flow field configuration but at the cost of higher-pressure drop. While three-dimensional theoretical models have been developed, the details of the flow field and pressure drop characteristics have not been studied systematically. The main objective of the present work is to use computational fluid dynamics (CFD)-based simulations to study the flow field in these channels under non-reacting conditions with a view to capturing the effect of important geometric parameters such as the channel, the header and the electrode dimensions. To this end, a number of calculations of the flow field have been carried out in a unit cell consisting of one inlet leg and one outlet leg connected to the corresponding headers. Additional calculations have been carried out in parallel configurations consisting of four and eight such unit cells. These calculations show the possibility of flow maldistribution under certain conditions. Details of the study and the results are discussed below.

2. Problem formulation

2.1. Methodology

The present calculation methodology is based on CFD simulations in which the fundamental equations governing the flow, namely, conservation of mass and conservation of momentum for an incompressible isothermal flow are solved numerically. CFD simulations have previously been used, including by the present authors (see, for example, [3,4,13,14]), to study different aspects of fuel cells-related flows. In the present study, the objective is to characterize the single-phase laminar flow through typical fuel cell gas distributor plates and gas diffusion layers (GDE) using an interdigitated flow field configuration. This is done by a two-pronged approach:

- In the first phase, the flow through a unit cell, consisting of one inlet gas distributor, one outlet gas distributor channel and the porous electrode connecting two, is analyzed for parametric dependence of the flow characteristics.
- In the second phase, the flow through a number of such unit cells are connected together through common headers is analyzed to model the flow in a gas distributor plate of interdigitated flow field configuration.

Care has been taken to make the dimensions, flow rates, etc. representative of typical fuel cell applications.

2.2. Governing equations

The governing equations, assuming steady incompressible flow of a Newtonian fluid, are the conservation of mass and momentum equations:

Mass balance equation:

$$\nabla(\rho V) = 0 \tag{1}$$

Momentum balance equation:

$$\nabla(\rho V \otimes V) = -\nabla(p\delta + \mu(\nabla V + (\nabla V)^{\mathrm{T}})) + S_{\mathrm{M}} \tag{2}$$

Here, V is the component of velocity, p the static pressure, ρ and μ are the fluid density and dynamic viscosity, respectively, δ the Kronecker delta. The term S_{M} appearing in the momentum balance equation is a momentum source term and is equal to zero for flow in the non-porous gas channels. For the porous gas diffusion electrodes (GDE), it is given by:

$$S_{\mathrm{M}} = -C_{\mathrm{Rl}} V \tag{3}$$

where C_{Rl} is the linear resistance coefficient and is given by:

$$C_{\mathrm{Rl}} = \frac{\mu}{K} \tag{4}$$

where μ is the absolute viscosity and K the permeability of the porous electrode. Thus, a Darcy-type of formulation is used here for flow through porous media. Since the Reynolds numbers are small and the porosity is isotropic in typical fuel cell applications, this treatment is expected to be adequate. The boundary conditions imposed are:

- Normal velocity specified as the mean flow velocity at the upstream "inlet".
- Fully developed flow condition specified at the downstream "outlet".
- No-slip condition (zero velocity for normal and tangential velocity components) on the side walls.

The nominal fluid properties correspond to those of air at atmospheric condition.

2.3. Solution method and validation

All the simulations were carried out using the commercial CFD code *CFX* version 5.7 of ANSYS, USA. It is a finite volume-based, unstructured grid, flow solver and can be used for a range of fluid flow applications. The overall accuracy of the discretization of the equations is nominally second order-accurate. A residual reduction factor of 10^{-8} for the mass conservation equation has been used to monitor the convergence of the iterative scheme.

The validation of the present calculation methodology is provided by comparing with the experimental results of Dohle et al. [15] who measured the pressure drop for a given volumetric flow rate for radially outward flow through a porous disk of thickness *s*. In the experimental set-up, the porous material sample is mounted between two end-plates made of perspex. The fluid enters through a central hole of radius R_{in} (see Fig. 2a) and is forced out radially through the disk of outer radius of R_{out}. The thickness of the diffusion layer is adjusted by distance spacers. The flow velocity passing through the porous diffusion layer and the pressure drop across the porous layer are related by Darcy's law. From measured values of the volumetric flow rate and the radial pressure drop, the permeability, K, can be calculated as:

$$K = \frac{Q}{\Delta P} = \frac{\mu}{2\pi s} \ln\left(\frac{R_{out}}{R_{in}}\right)$$

where ΔP is pressure drop in the diffusion layer and Q volumetric flow rate.

CFD-based simulations were carried out to calculate the pressure drop in the porous diffusion plate of same dimensions as used by Dohle et al. [15]. Taking advantage of symmetry, simulations were conducted for one quarter of the set-up (see Fig. 2b). The permeability determined by Dohle et al. has been used in the simulations to calculate the overall pressure drop in the diffusion layer for a given volumetric flow rate. As expected, the flow was found to be essentially radial. Since the flow cross-sectional area increases in the flow direction, the mean velocity varies as r^{-1}. For the laminar flow cases investigated, the pressure also showed a similar relationship, which is to be expected. The pressure drop between the inlet and the outlet for a given volumetric flow rate obtained from CFD-simulations are compared in Fig. 2c with those measured by Dohle et al. [15]. Excellent agreement is obtained between the two for the two disk thicknesses used in the experiments. This validates the treatment of porous medium flow used in the CFD simulations.

3. Results from the unit cell calculations

The flow geometry considered in these calculations is shown schematically in Fig. 3. It consists of two straight channels of length L_c, width W_c and height H_c, one of which acts as the inlet and the other as the outlet for the flow of gaseous reactants/products. The two channels are separated by a distance W_r. The flow path between the two is completed by the porous electrode of thickness s and permeability K. Thus, the gas enters the inlet channel from the inlet header (not shown

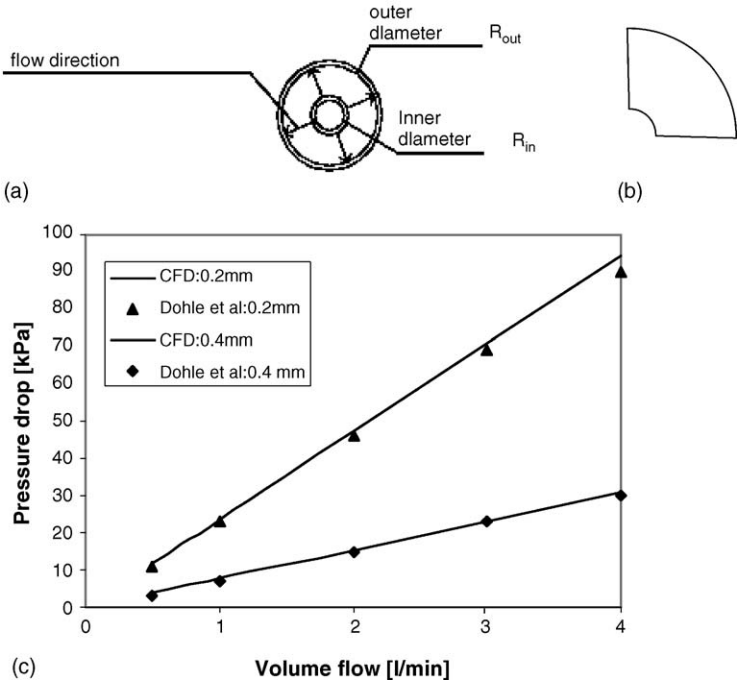

Fig. 2. (a) Experimental setup of Dohle et al. [15]; (b) flow geometry used in CFD simulations; and (c) comparison of the predicted and the measured pressure drop as a function of the volumetric flow rate.

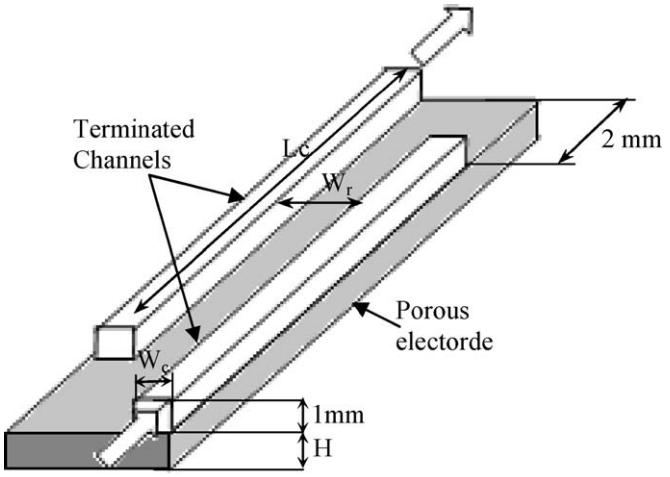

Fig. 3. A single pair (unit cell) of interdigitated flow field with parameters and dimensions.

in Fig. 3), diffuses through the porous electrode to enter the outlet channel and is eventually evacuated by the outlet header. The values of the channel and electrode dimensions and flow properties used in the present study are typical of those used in earlier studies of interdigitated channels [3–12] and are listed in Table 1. A detailed study of the flow within these and the effect of the geometric and flow parameters thereon are discussed below.

Typical flow field for a unit cell is shown in Fig. 4 in the form of contours of velocity and pressure at mid-plane of the gas channels for two permeability values, namely, for a high permeability of 10^{-10} m^2 and for a low permeability of 10^{-14} m^2. It can be seen from the velocity contour plots (Fig. 4a) that the flow goes from the inlet section to the outlet section all along the common length the of gas channel sections. Thus, the inlet channel shows a decreasing velocity at the mid-plane along the length while the outlet channel shows a corresponding increase. The pressure contours for the low permeability case (Fig. 4b(ii)) show virtually no variation of pressure along the length of the channel while at high permeability values (Fig. 4b(i)) a gradual decrease in pressure can be seen in the flow direction in the two sections. The velocity contours in the mid-plane of the electrode are drawn in Fig. 4c for the two permeabilities. At high permeabilities (Fig. 4c(i)), the flow distribution along the length is non-uniform. Also to be noted in both cases is the leakage of flow into the gas channels through the side wall of the porous medium. The variation along the length of the velocity at mid-height of the electrode, made dimensionless by dividing

Table 1
Parameters used for the characterization of single pair of interdigitated channels

Rib width between channels, W_r (mm)	1, 1.5, 2, 2.5
Thickness of the electrode, H (mm)	0.1, 0.15, 0.2, 0.25
Permeability (m^2)	5E-10, 1E-10, 8E-11, 5E-11, 1E-11, 1E-12, 1E-13, 1E-14
Reynolds number	100–2000
Length of the channel, L_c (mm)	48
Channel width, W_c (mm)	2

Table 2
Base case conditions for a pair of interdigitated channel

Rib width between channels, W_r (mm)	2.5
Thickness of the electrode, H (mm)	0.2
Permeability (m^2)	1E-10
Reynolds number	443
Length of the channel, L_c (mm)	48
Channel width, W_c (mm)	2

the mean velocity, is shown in Fig. 4d for low and high permeability cases. In the case of the former, a uniform velocity is obtained throughout except at the two ends where some leakage flow occurs. In the high permeability case, the flow rate is clearly non-uniform. Thus, the flow in the porous medium can be three-dimensional and uniformity of the flow cannot be expected at high permeabilities.

3.1. Effect of rib width

Increasing the rib width has the effect of increasing the resistance for flow between the inlet and the outlet gas channels. This would tend to increase the pressure drop. As already seen from Fig. 4 above, for small permeabilities, the flow across the channels is uniform and that it is not so at high values of permeability. Fig. 5a shows the pressure drop between the entrance of the inlet gas channel and the exit of the outlet gas channel for the base case (see Table 2) with a rib width of 2 mm at a Reynolds number of 443 and for a high permeability of $K = 10^{-10}$ m^2. The pressure difference between the inlet and the outlet varies along the distance indicating flow non-uniformity. Increasing the rib width while keeping everything else the same increases the overall pressure drop which has the effect of making the flow more uniform. The overall pressure drop between the entrance and the exit varies nearly linearly with the rib width as shown in Fig. 5b even at the high value of K. This shows that the source term in the momentum balance Eq. (4) is the dominant term and that the inertial effects are of minor importance. The overall pressure drop is therefore determined by the traversed distance in the porous medium section of the distributor plate.

3.2. Effect of electrode thickness

Increasing the electrode thickness while keeping other parameters constant increases the flow cross-sectional area through the porous medium and therefore reduces the mean velocity of the fluid. Since the overall pressure drop in predominantly due to that across the porous section and since this pressure drop is directly proportional to the mean velocity through Darcy's relation (see Eq. (4)), one would expect the overall pressure drop to vary inversely with the electrode thickness. The results from the CFD simulations for different electrode thicknesses in the range of 0.1–0.25 mm for permeability values in the range of 10^{-11} to 10^{-10} m^2 confirm this trend (Fig. 6). It is also important to note that, since the pressure drop decreases as the electrode thickness increases, it is possible for the flow distribution to be affected. Indeed, it was

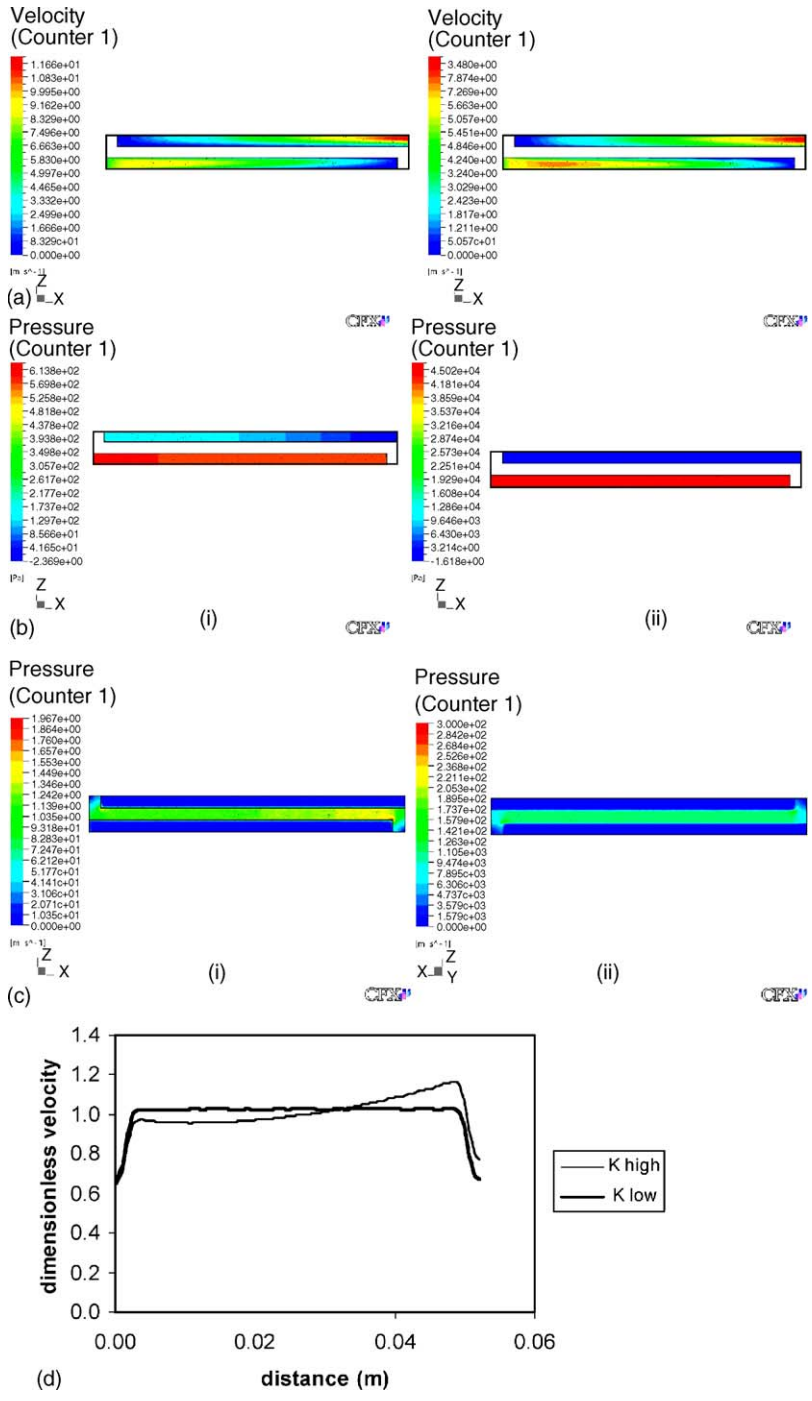

Fig. 4. (a) Velocity contours for a permeability of: (i) 10^{-10} and (ii) 10^{-14} m^2 in the channels in a plane at $y = 0.5$ mm. (b) Pressure contours for a permeability of: (i) 10^{-10} and (ii) 10^{-14} m^2 in the channels in a plane at $y = 0.5$ mm. (c) Velocity contour for a permeability of 10^{-10} and 10^{-14} m^2 in the electrode in a plane at $y = 1.1$ mm. (d) Dimensionless velocity variation along the distance at mid-height of the electrode for low (10^{-14} m^2) and high (10^{-10} m^2) permeabilities.

observed that the flow distribution along the channel length was more uniform for an electrode thickness of 0.1 mm than for 0.25 mm. This shows that a thicker electrode would be better from the point of view of lower pressure drop but may have the undesirable consequence of increased flow non-uniformity and increased mass transfer for the transport of the reactants and products (besides being bulky). There is a possibility of optimization of electrode thickness for overall efficiency of the fuel cell.

3.3. Effect of electrode permeability

The permeability of the electrode depends on the electrode material and its characteristics. It is also one of the important parameters to affect the overall pressure drop in the interdigitated flow field configuration. The predicted pressure variation in the inlet and the outlet gas channels for various values of the permeability is shown in Fig. 7. For low values of K, i.e. for $K = 10^{-14}$ and 10^{-11} m^2 in Fig. 7, there is negligible variation

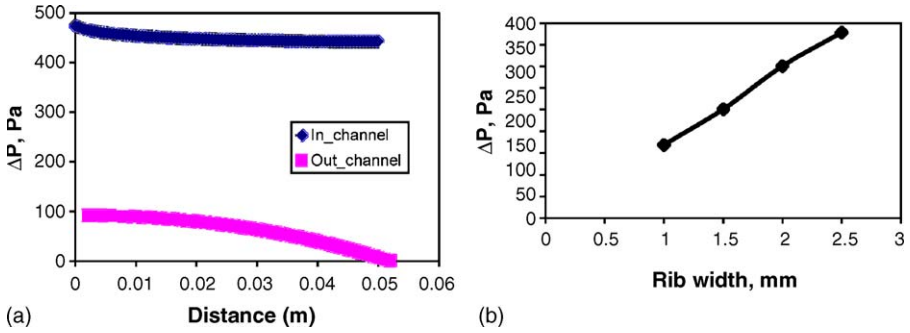

Fig. 5. (a) Pressure variation along the length of the inlet and outlet channel for the base case. (b) Pressure drop for different rib widths.

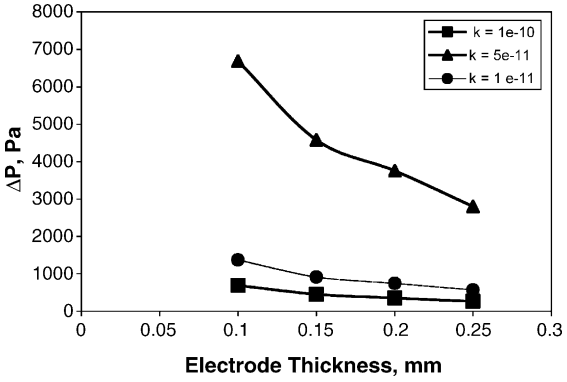

Fig. 6. Pressure drop for different electrode thickness at different permeabilities.

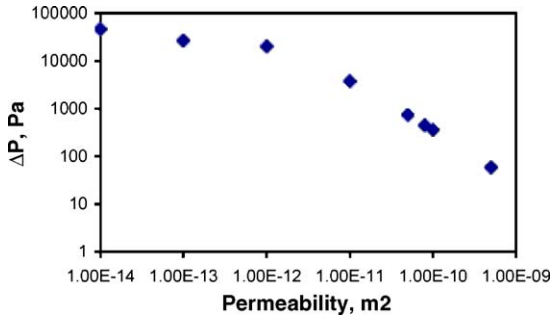

Fig. 8. Variation of pressure drop for different permeabilities.

along the channel length and the pressure drop and hence the flow rate is constant. At higher values, i.e. for $K = 8 \times 10^{-11}$ m^2, there is an appreciable variation in the pressure along the channel while for $K = 10^{-10}$ m^2, severe maldistribution of flow across the electrode may occur. The calculated pressure drop between the entrance and the exit to the plate is plotted in Fig. 8 for different values of K at a Reynolds number of 443. This shows that there is considerable decrease in the pressure drop (by orders of magnitude) at high K. However, increasing the permeability to reduce the pressure drop may result in flow non-uniformity in the distributor plate. An optimum value of K must therefore be chosen.

3.4. Effect of Reynolds number

The overall pressure drop between the entrance and the exit of the unit cell varies linearly with Reynolds number as shown in Fig. 9a for a permeability value of 10^{-10} m^2. This shows

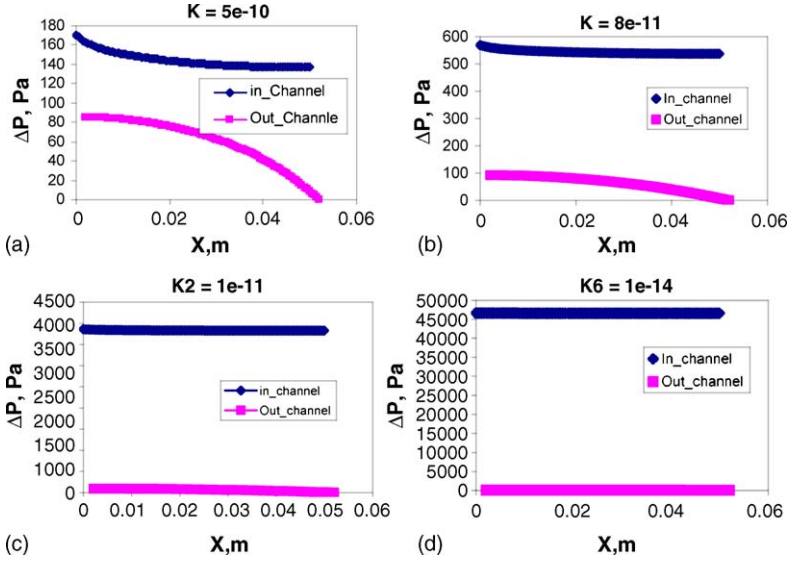

Fig. 7. Pressure distribution along the length of the inlet and outlet channel of the interdigitated flow field for permeabilities of: (a) 5×10^{-10}; (b) 8×10^{-11}; (c) 10^{-11}; and (d) 10^{-14} m^2.

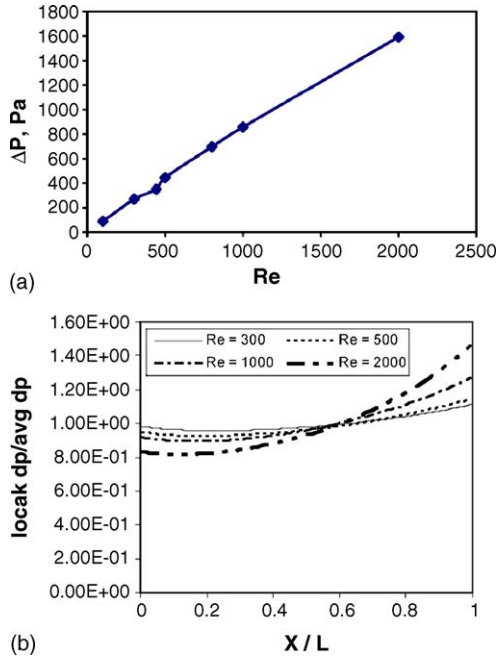

Fig. 9. (a) Effect of Reynolds number on pressure drop. (b) Non-dimensionalized local pressure difference vs. dimensionless length for different *Re*.

the pressure gradient is more or less determined by the pressure drop across the porous electrode. However, the variation of the local pressure difference between the inlet and the outlet, which determines the local flow rate through the porous electrode, shows a more complicated dependence on the Reynolds number. As shown in Fig. 9b, where the local pressure difference non-dimensionalized by the average pressure difference is plotted along the dimensionless length, severe non-uniformity of flow may be expected at high *Re*.

The above results show that while uniform flow distribution may be expected for low values of permeability, non-uniform distribution of reactants may occur when the permeability is of the order of 10^{-10} m^2 for typical distributor plate dimensions and flow rates.

4. Results from multiple interdigitated channels

In order to investigate the effect of a number of parallel channels of interdigitated configuration on the flow field, calculations have been made for two configurations: a four-cell unit (Fig. 10a) and an eight-cell unit (Fig. 10b). The dimensions of the channels, etc. are the same as those for the unit cell except for the common inlet and outlet headers, both of which are of a width of 4 mm (Table 3). Calculations were made in the header Reynolds

Table 3
Base case conditions for multiple interdigitated channels

Header dimensions (mm)	Width, $W_h = 4$; height, $H_h = 1$
Channel dimensions (mm)	Width, $W_c = 2$; height, $H_c = 1$; length, $L_c = 100$
Rib width, W_r (mm)	2
Permeability (m^2)	1×10^{-11}
Electrode	Thickness = 0.2

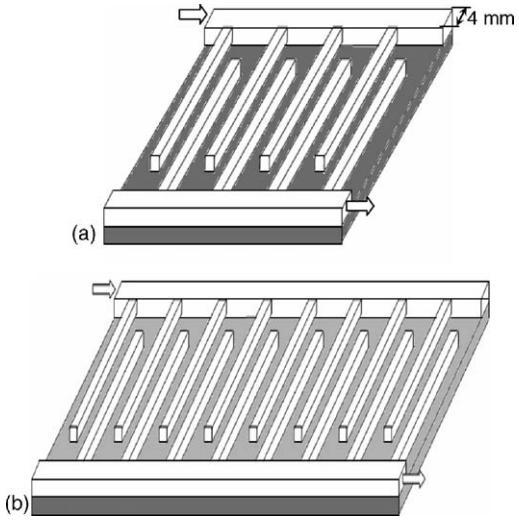

Fig. 10. (a) Details of a four pair interdigitated flow field. Only the header width is indicated, all other parameters are same as the unit cell shown in Fig. 3. (b) An eight-cell interdigitated flow field.

number range of 300–1600, electrode permeabilities of 10^{-11} and 10^{-10} m^2 and electrode thicknesses of 0.2 and 0.3 mm. For the four-channel configuration, both *U*-type and *Z*-type arrangement [4] of the parallel channels was considered. In the *U*-type, both the inlet and the outlet are located on the same side in a two-dimensional representation of the flow field while in the *Z*-type, they are located in the opposite sides.

The predicted velocity contours in the mid-plane of the electrode of a thickness of 0.2 mm with a permeability of 10^{-10} m^2 for a Reynolds number of 1600 based on the inlet header dimensions and mean velocity are shown in Fig. 11 for the four-cell *U*-type, the four-cell *Z*-type and the eight-cell *Z*-type configurations. Because of the fairly large pressure drop between the gas channel and the porous electrode, the flow in the porous medium at the ends of the channel becomes three-dimensional, as remarked earlier, and some flow occurs through the sides of the gas channel also. This gives the appearance of a serpentine flow configuration within the porous electrode as can be seen clearly in Fig. 11. Another distinguishing feature of a multi-cell interdigitated configuration is that an interior inlet leg can feed, through the porous electrode, to the two neighbouring outlet legs and similarly an interior outlet leg can draw unspent reactants or products from two neighbouring inlet legs. This would promote a more equitable distribution of the fluid in all the legs of a multi-cell distributor plate. In spite of this, one notices significant maldistribution of the flow in Fig. 11 through the four-cell and the eight-cell configurations.

The relative flow distribution among the channels is plotted in Fig. 12 as a function of the header Reynolds number. The relative flow rate in the inlet and the outlet channels is given separately. It is seen that, for this *Z*-type arrangement, among the interior channels, the flow rate is minimum for the central channels, which is to be expected [4]. This is true for both the set of inlet and the set of outlet channels. However, the flow rate in the extreme channels, i.e. in the first channel of the inlet header and in the eighth channel of the outlet header, the flow distribution

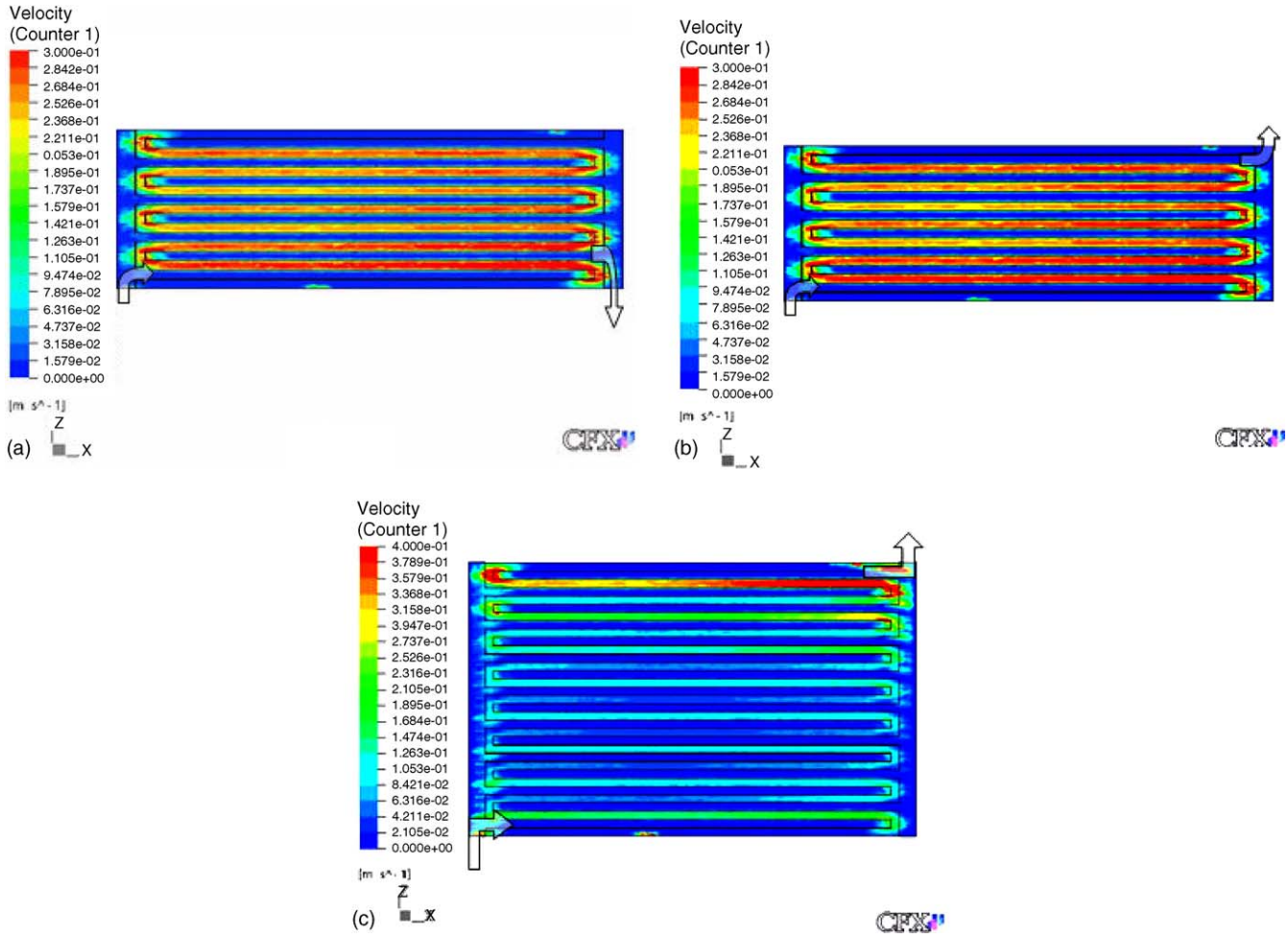

Fig. 11. Velocity contours at the mid-plane of the electrode for: (a) the four-cell *U*-type, (b) the four-cell *Z*-type and (c) the eight-cell *Z*-type configurations.

is affected by the end conditions. The first channel of the inlet header has only one outlet channel to feed to (compared to the second inlet channel which has two outlet channels, namely, the first and the second outlet channels to feed to), and, as a result, the flow rate through it is less. Similarly, the eighth channel of the outlet header has only one channel, namely, the eighth channel of the inlet header, to receive flow from (compared to the seventh outlet channel which can receive flow from both the seventh and the eighth inlet channels), and therefore has less flow rate than its neighbour.

The relative flow distribution in a set of parallel channels can be measured by the flow non-uniformity index [16,4] defined as:

$$F = \frac{m'_{\mathrm{c,max}} - m'_{\mathrm{c,min}}}{m'_{\mathrm{c,max}}}$$

where $m'_{\mathrm{c,max}}$ and $m'_{\mathrm{c,min}}$ are the maximum and minimum flow rates in a set of parallel channels. A low value of F indicates uniform flow (when $F=0$, the flow rate is identical in all the channels). Computed values of the flow non-uniformity index are listed in Table 4 for several combinations of the number of cells, permeability and electrode thickness. It can be seen that the flow non-uniformity increases as the Reynolds number increases, which is also evident from Fig. 12. Increasing the number of parallel channels reduces the flow rate through the individual channels and the pressure drop in the electrodes is correspondingly less. This has the tendency to increase the flow non-uniformity. Increasing the permeability or the electrode thickness also has the tendency to reduce pressure drop in the electrode and therefore leads to increased flow maldistribution. Generally speaking, the flow non-uniformity index in the set of inlet and the set of outlet channels is not the same. The decreased flow rate in the first channel of the inlet header has the effect of accentuating the flow non-uniformity while the decreased flow rate in the last channel of the outlet header has the effect of mitigating the flow maldistribution.

The overall pressure drop, i.e. the pressure drop between the entrance and the exit of the distributor plate, for the eight-cell configuration is less than that for a unit-cell configuration for the same volumetric flow rate because the flow rate in the individual channels is less by a factor N, where N is the number of parallel channels. Since the pressure drop in an interdigitated flow field is mainly due to the pressure drop in the electrode, the overall pressure drop is expected is decrease by a factor of N. However, for high permeabilities, one may expect significant pressure losses in the headers also. The flow distribution is also likely to be

Table 4
Flow non uniformity index for different multiple interdigitated channel configuration at different Reynolds number

Permeability, K (m^2)	Flow configuration	Electrode thickness (mm)	Re	Flow non-uniformity index, F	
				F_{in}	F_{out}
lE-11	4-*Z*	0.2	300	0.342	0.248
lE-11	4-*Z*	0.2	600	0.365	0.222
lE-11	4-*Z*	0.2	1000	0.391	0.188
lE-11	4-*Z*	0.2	1600	0.43	0.14
lE-11	4-*U*	0.2	300	0.291	0.333
lE-11	4-*U*	0.2	600	0.277	0.327
lE-11	4-*U*	0.2	1000	0.261	0.318
lE-11	4-*U*	0.2	1600	0.239	0.309
lE-10	8-*Z*	0.2	300	0.49	0.398
lE-10	8-*Z*	0.2	600	0.591	0.539
lE-10	8-*Z*	0.2	1000	0.685	0.643
lE-10	8-*Z*	0.2	1600	0.759	0.72
lE-11	8-*Z*	0.2	300	0.393	0.21
lE-11	8-*Z*	0.2	600	0.442	0.19
lE-11	8-*Z*	0.2	1000	0.469	0.242
lE-11	8-*Z*	0.2	1600	0.548	0.323
lE-11	8-*Z*	0.3	300	0.419	0.229
lE-11	8-*Z*	0.3	600	0.48	0.21
lE-11	8-*Z*	0.3	1000	0.524	0.254
lE-11	8-*Z*	0.3	1600	0.579	0.341

non-uniform and one may not realize a factor of N decrease in the pressure drop. This is shown to be the case in Fig. 13a where the computed pressure drop is shown for a unit-cell and an eight-cell configuration for the same volumetric flow rate for different header Reynolds numbers and for an electrode permeability of 10^{-10} m^2. While the unit-cell pressure drop shows a linear increase with Reynolds number, the eight-cell pressure drop shows a more-than linear variation. The predicted pressure drop variation with Reynolds number for the eight-cell configuration is compared in Fig. 13b for permeabilities of 10^{-11} and 10^{-10} m^2. These show that the pressure drop varies as $\sim Re^{1.2}$ and $\sim Re^{1.4}$, respectively, showing increasingly non-linear variation at higher permeabilities. This can be attributed to the flow maldistribution among the parallel channels.

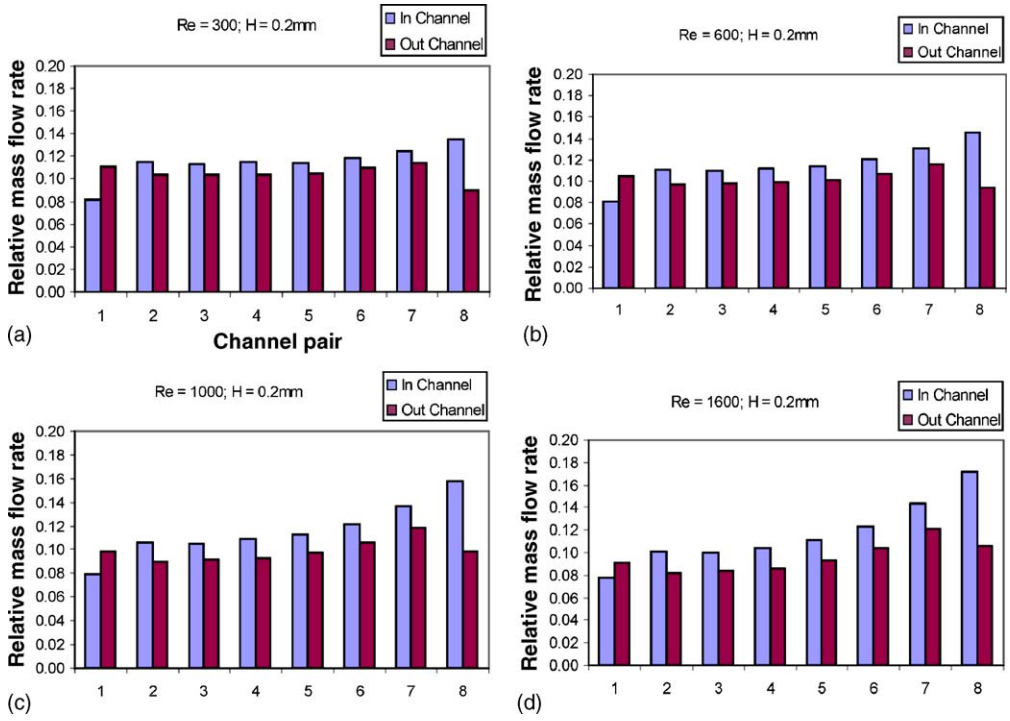

Fig. 12. Relative mass flow rate in different in- and out-channels of the interdigitated flow field for a header Reynolds number of: (a) 300; (b) 600; (c) 1000; and (d) 1600.

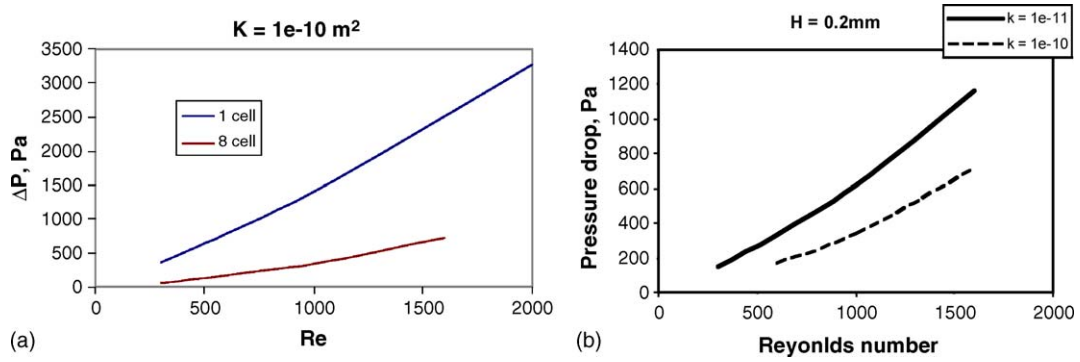

Fig. 13. (a) Pressure drop in the unit-cell and the eight-cell configurations as a function of the header Reynolds numbers for a permeability of 10^{-10} m^2. (b) Comparison of the pressure drop in the eight-cell configuration for permeabilities of 10^{-10} and 10^{-11} m^2.

5. Conclusion

Interdigitated flow fields are used for the better distribution of the reactants across the electrode diffusion layer by convection rather than by diffusion. The results from the present CFD simulations show that flow non-uniformity even in a single pair of inlet–electrode–outlet channel configuration is not likely for high permeabilities, typically of the order of 10^{-11} to 10^{-10} m^2. For lower values of permeabilities, the flow can be expected to be uniform and the pressure drop is given primarily by the traversed length in the electrode region. For multiple channel configurations such as the four-cell and the eight-cell configurations studied here, significant flow non-uniformity is likely in different legs for permeabilities in the range of 10^{-11} to 10^{-10} m^2. Any measures that tend to decrease the pressure drop, such as increasing the electrode width, increasing the number of parallel channels, increasing the permeability, have the tendency to increase flow non-uniformity. Selection of the geometric and flow parameters of the interdigitated channels has to be done carefully to minimize flow maldistribution.

References

[1] X. Li, I. Sabir, Review of bipolar plates in PEM fuel cells: Flow-field designs, Int. J. Hydrogen Energy 30 (2005) 359–371.
[2] A. Biyikõglu, Review of proton exchange membrane fuel cell models, Int. J. Hydrogen Energy 30 (2005) 1181–1212.
[3] S. Maharudrayya, S. Jayanti, A.P. Deshpande, Pressure losses in laminar flow through serpentine channels in fuel cell stacks, J. Power Sources 138 (2004) 1–13.
[4] S. Maharudrayya, S. Jayanti, A.P. Deshpande, Flow distribution and pressure drop in parallel-channel configurations of planar fuel cells, J. Power Sources 144 (2005) 94–106.
[5] T.V. Nguyen, A gas distributor design for proton-exchange-membrane fuel cells, J. Electrochem. Soc. 143 (1996) L103–L105.
[6] D.L. Wood III., J.S. Yi, T.V. Nguyen, Effect of direct liquid water injection and interdigitated flow field on the performance of proton exchange membrane fuel cells, Electrochim. Acta 43 (1998) 3795–3809.
[7] S. Yi, T.V. Nguyen, Multicomponent transport in porous electrodes of proton exchange membrane fuel cells using the interdigitated gas distributors, J. Electrochem. Soc. 146 (1999) 38–45.
[8] W. He, J.S. Yi, T.V. Nguyen, Two-phase flow model of the cathode of PEM fuel cells using interdigitated flow fields, AlChE J. 46 (2000) 2053–2064.
[9] A. De Souza, E.R. Gonalez, Influence of the operational parameters on the performance of the polymer electrolyte membrane fuel cells with different flow fields, J. Solid State Electrochem. 7 (2003) 651–657.
[10] L. Wang, H. Liu, Performance studies of PEM fuel cells with interdigitated flow fields, J. Power Sources 134 (2004) 185–196.
[11] G. Hu, J. Fan, S. Chen, Y. Liu, K. Cen, Three-dimensional numerical analysis of proton exchange membrane fuel cells with conventional and interdigitated flow fields, J. Power Sources 136 (2004) 1–9.
[12] M. Grujicic, C.L. Zhao, K.M. Chittajallu, J.M. Ochterbeck, Cathode and interdigitated air distributor geometry optimization in polymer electrolyte membrane (PEM) fuel cells, Mater. Sci. Eng. 108 (2004) 241–252.
[13] T. Berning, D.M. Lu, N. Djilali, Three-dimensional computational analysis of transport in a PEM fuel cell, J. Power Sources 106 (2002) 284–294.
[14] S. Um, C.Y. Wang, Three-dimensional analysis of transport and electrochemical reactions in polymer electrolyte fuel cells, J. Power Sources 125 (2004) 40–51.
[15] H. Dohle, R. Jung, N. Kimiaie, J. Muller, Interaction between the diffusion layer and the flow field of polymer electrolyte membrane fuel cells: experiments and simulation studies, J. Power Sources 124 (2003) 371–384.
[16] J.R. Kee, P. Korada, K. Walters, M. Pavol, A generalized model of the flow distribution in channel networks of planar fuel cells, J. Power Sources 109 (2002) 148–159.